Talanta 119 (2014) 207–213

Contents lists available at ScienceDirect

Talanta

journal homepage: www.elsevier.com/locate/talanta

A flower-like nickel oxide nanostructure: Synthesis and application for choline sensing

N. Sattarahmady [a,c,d], H. Heli [b,c,d,*], R. Dehdari Vais [b,c]

[a] Pharmaceutical Science Research Center, School of Pharmacy, Shiraz University of Medical Sciences, Shiraz, Iran
[b] Nanomedicine and Nanobiology Research Center, Shiraz University of Medical Sciences, Shiraz, Iran
[c] Department of Medical Physics, School of Medicine, Shiraz University of Medical Sciences, Shiraz, Iran
[d] Department of Nanomedicine, School of Advanced Medical Sciences and Technologies, Shiraz University of Medical Sciences, Shiraz, Iran

ARTICLE INFO

Article history:
Received 25 June 2013
Received in revised form
2 November 2013
Accepted 4 November 2013
Available online 11 November 2013

Keywords:
Choline
Nickel oxide
Flower-like nanostructure
Electrocatalysis
Nanobiosensor

ABSTRACT

Flower-like nickel oxide nanostructure was synthesized by a simple desolvation method. The nanostructure was then employed as the modifier of a carbon paste electrode to fabricate a choline sensor. The mechanism and kinetics of the electrocatalytic oxidation of choline on the modified electrode surface were studied by cyclic voltammetry, steady-state polarization curve, and chronoamperometry. The catalytic rate constant and the charge transfer coefficient of the choline electrooxidation process by an active nickel species, and the diffusion coefficient of choline were reported. An amperometric method was developed for determination of choline with a sensitivity of 60.5 mA mol^{-1} L cm^{-2} and a limit of detection of 25.4 μmol L^{-1}. The sensor had the advantages of high electrocatalytic activity and sensitivity, and long-term stability toward choline, with a simple fabrication method without complications of immobilization steps and using any enzyme or reagent.

1. Introduction

Conductive metal oxides have been of tremendous interest in researches, fabrication of devices and industrial applications due to their excellent electrochemical behavior. Among these metal oxides, there are great scientific and technological interests in the synthesis of nickel (hydr)oxide due to its applications in different electrochemical devices, such as electrocatalysts [1], sensors and biosensors [2,3], and accumulators [4]. The main reasons for these utilities are the conductivity (as a p-type semiconductor with a wide band-gap energy range), high specific energy, low cost, chemical and electrochemical stabilities, outstanding durability, near-reversible redox properties, large span optical density and electrochromic properties, and high resistance to anodic corrosion of this compound [1–5].

The ability to tune the size, shape and structure of transition metals is an important goal in the current material synthesis, and there has been increasing interested in the synthesis of nanostructures of transition metal compounds with special shape and structure [3,6–13]. This is due to their potential applications in catalysts and electrocatalysts, sensors and biosensors, photonics and optoelectronics, drug delivery and formulation, biomedical diagnostics, treatment and equipment, and energy producing and accumulating devices [6–14]. Among the numerous approaches used to fabricate these materials, those resulting in the production of flower-like nanostructures have been greatly approached due to interesting structure, shape and properties [6,15–17].

The physical and chemical properties of nickel (hydr)oxide nanostructures strongly depend on their size and shape. So far, nanoflakes and nanoplatelet [18–20], nanotubes [11,21], hollow spheres [22], nanowires [23], nanoparticles [24], nanoribbons [25] and nanoflowers [26] of nickel oxide have been synthesized.

Choline, as a vitamin-like compound, is a water-soluble essential nutrient. It is the metabolite of the neurotransmitter acetylcholine which plays vital roles in maintaining the central nervous system and numerous metabolic functions. Choline is a precursor of the synthesis of acetylcholine, cell-membrane lipid phosphatidylcholine and betaine [27]. Therefore, it is important for the integrity of cell membranes, lipid metabolism, and cholinergic nerve function [28,29]. The dietary availability of choline affects the apoptotic signaling in the neurons and liver cells, neural tube closure and hippocampal cholinergic development and hepatic transport of lipoproteins [30]. It seems that the choline brain level causes various neural disorders such as Alzheimer's disease, progressive dementia [31–34], and schizophrenia [35]. Choline deficiency can also lead to carcinogenesis [36]. Therefore, development of sensitive and accurate measurement methods of choline is important. On the other hand, choline does not bear chromophore, flourophore or electroreactive functional groups.

* Corresponding author at: Nanomedicine and Nanobiology Research Center, Shiraz University of Medical Sciences, Shiraz, Iran. Tel./fax: +98 711 234 93 32.
E-mail addresses: hheli7@yahoo.com, heli@sums.ac.ir (H. Heli).

0039-9140/$ - see front matter © 2013 Elsevier B.V. All rights reserved.
http://dx.doi.org/10.1016/j.talanta.2013.11.002

Therefore, well established methods typically employed for the analysis of biologically important compounds are useless, and a pre-derivatization procedure into more easily detectable compounds is usually required. In this regard, the most successful approaches for choline determination have been based on liquid chromatography (LC) coupled with post-column enzymatic conversion [37] or immobilized on suitable enzyme reactors [38–44]. These methods are tedious and time-consuming, and suffer from some drawbacks such as loss of chromatographic resolution and peak tailing or splitting. In addition, several amperometric biosensors based on immobilized choline oxidase have been reported [45–47]. However, serious enzyme immobilizing procedure, poor stability and enzyme loss are the main disadvantages. Radioenzymatic and chemiluminescent assays [48], ^{1}H-NMR [49] and liquid chromatography-isotope dilution mass spectrometry [50] which are high-cost techniques and need pre-processing steps of extraction and derivatization have also been reported for choline determination.

In the present study, flower-like nickel oxide nanostructure was synthesized and then employed to modify a carbon paste electrode. The electrochemical kinetics of the modified electrode was studied and finally applied to the electrocatalytic oxidation and sensing of choline.

2. Experimental section

2.1. Materials and synthesis procedures

Graphite fine powder with a particle size of $<50\,\mu m$ was obtained from Merck. All other chemicals were of analytical grade from Merck or Sigma and used without further purification. All solutions were prepared with doubly distilled water.

Flower-like nickel oxide nanostructure was synthesized by a nickel complex decomposition-precipitation method. In a typical procedure, 291 mg $Ni(NO_3)_2 \cdot 6\,H_2O$ was dissolved in 10 mL water. Then, concentrated ammonia solution was added until formation of $Ni(OH)_2$. The precipitate color was light green. Addition of ammonia solution was continued just to dissolve $Ni(OH)_2$ and form dark blue nickel-ammonia complex with a solution pH of ≈ 10. This solution was then placed near a baker containing 10 mL concentrated sulfuric acid in a closed polyethylene container for 48 h at room temperature. A light green powder was so precipitated. The product was washed with distilled water and ethanol and dried at 40 °C to obtain the nickel oxide nanostructure.

2.2. Working electrodes

Carbon paste electrode (CPE) was prepared by hand-mixing graphite fine powder and mineral oil with a ratio of 80/20% (w/w). The paste was packed firmly into a cavity (2 mm diameter) at the end of a Teflon tube. Electrical contact was established by a copper wire.

Modified carbon paste electrodes with flower-like nickel oxide nanostructure (MCPE) were prepared by mixing graphite fine powder, mineral oil, and flower-like nickel oxide nanostructure with ratios of 60:20:20 by wt%. In order to cover the MCPE surface with a Nafion layer, 10 μL of a 2% w/v low aliphatic alcohols Nafion solution was dropped on the electrode surface and placed under an IR lamp to dry.

Before performing any experiment, MCPE was transferred to a 100 mmol L^{-1} NaOH solution (the supporting electrolyte) and 25 potential cycles were applied in a regime of cyclic voltammetry in the potential range of −200 to 800 mV at a potential sweep rate of 50 mV s^{-1}. This procedure caused the voltammograms of MCPE to become more stable and reproducible.

2.3. Equipments and methods

All electrochemical studies were performed in a conventional three-electrode cell containing 100 mmol L^{-1} NaOH solution as the supporting electrolyte. μ-Autolab type III potentiostat/galvanostat (The Netherlands) was used. An Ag/AgCl, 3 mol L^{-1} KCl, and a platinum sheet were used as the reference and counter electrodes, respectively. The system was run on a PC through GPES 4.9 software.

Scanning electron microscopy (SEM) was performed using an X-30 Philips instrument. Powder X-ray diffraction (XRD) patterns were recorded in the 2θ range 10 to 9° at a scanning rate of 2.4° min^{-1} by an X-ray diffractometer (Philips X'Pert, The Netherlands) with a Cu Kα radiation at 40 kV and 30 mA. All measurements were carried out at room temperature.

3. Results and discussion

SEM images of the nickel oxide nanostructure with different magnifications are represented in Fig. 1. The images show irregular and assembled flakes of ≈ 30 nm thickness. These nanosheets are intertwined with each other and construct a porous flower-like nanostructure. The nanoflowers have a highly active surface area and aspect ratio whose internal parts may not be fully utilized. The electrolyte and electrolyte species would permeate into the nanostructure.

Typical powder XRD pattern of the nanoflowers is shown in Fig. 2. In this diffractogram, there are slightly broadened diffraction lines. Main diffraction peaks at 19.3°, 33.1°, 38.5°, 39.1°, 52.1°, 59.1°, 62.7° and 72.7° are indexed to (0 0 1), (1 0 0), (1 0 1), (0 0 2), (1 0 2), (1 1 0), (1 1 1) and (2 0 1) reflections, respectively. They are indexed to a hexagonal system with p-3m1 space group and space group number of 164 (Joint Committee on Powder Diffraction Standards, JCPDS Card no. 00-014-0117). The calculated lattice parameters of the nanoflowers are as follows: $a=3.1260$ Å, $b=3.1260$ Å, $c=4.6050$ Å, and $V=38.97$ Å^3.

Typical cyclic voltammogram of MCPE recorded in the supporting electrolyte with a potential sweep rate of 50 mV s^{-1} is shown in Fig. 3A. In this voltammogram, a pair of well-defined peak appears and the pattern of the voltammogram is similar to those previously reported [2,3,11]. The formal potential of the redox transition was estimated to be ≈ 400 mV (as an average mid peak of cyclic voltammograms recorded at slow potential sweep rates of <10 mV s^{-1}), and the ratio of the peak currents (I_{pa}/I_{pc}) was almost equal unity. The redox reaction in the voltammogram is attributed to the Ni(II)/Ni(III) transition at the MCPE surface via the following reaction [2,3,11,51]:

$$NiOOH + H_2O + e \rightleftarrows Ni(OH)_2 + OH^- \quad (1)$$

The anodic-to-cathodic peak potential difference in the voltammogram of MCPE is about 108 mV, at a potential sweep rate of 50 mV s^{-1}. This value is greater than that for immobilized (adsorbed) redox species of zero and also increases with the potential sweep rate increment. This indicates a limitation in the rate of charge transfer process due to one or some of the following reasons: limitation in the electronic conductivity of the MCPE bulk, interactions of electrolyte ions with the MCPE surface, the lateral interactions of the nickel sites at the MCPE surface, diffusion of ions in the MCPE bulk and its coupling with migration processes, and non-equivalency of redox sites at the MCPE surface. Another point in the voltammogram of MCPE is that the average value of full width at half height of anodic peak is about 32 mV. This value is less than the theoretical value of 90 mV for non-interacting one-electron surface redox sites [52]. It confirms domination of site–site attractions [53].

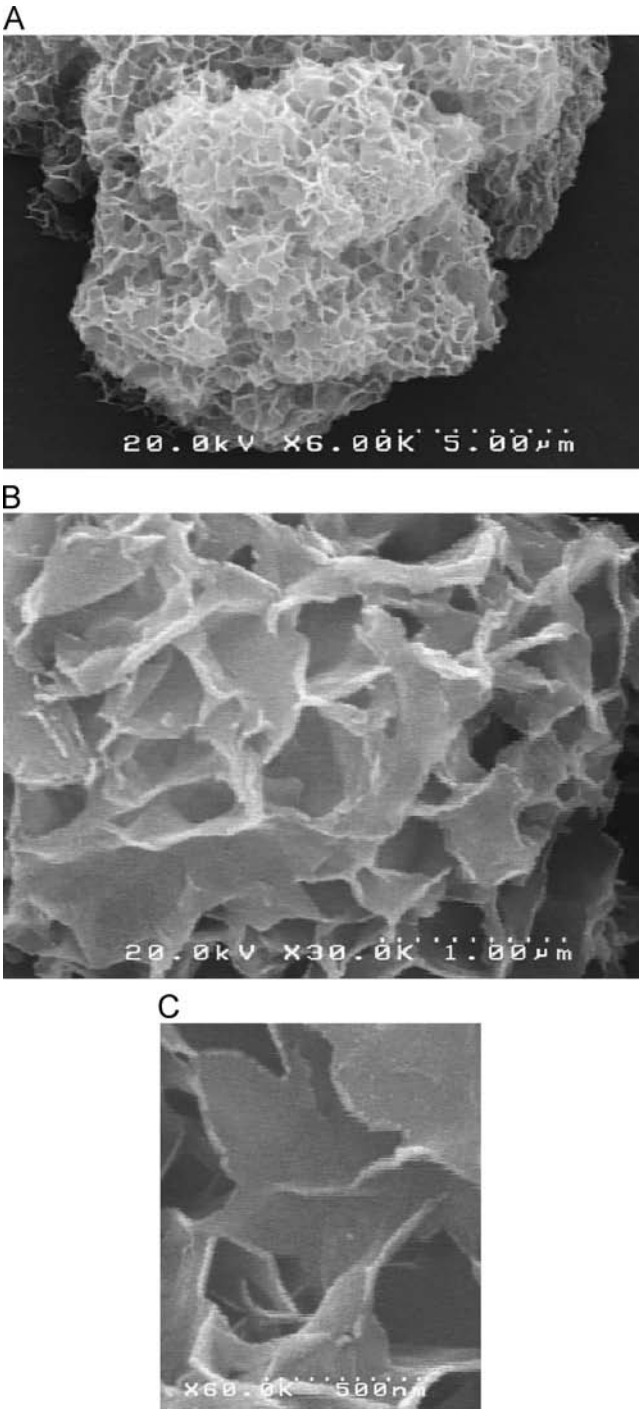

Fig. 1. SEM images of the flower-like nickel oxide nanostructure with different magnifications.

Cyclic voltammograms of MCPE recorded at different potential sweep rates (1–1000 mV s^{-1}) are shown in Fig. 3B. In these voltammograms, upon increasing in the potential sweep rate, the peak currents increased with the potential sweep rate and I_{pa}/I_{pc} remained almost constant and near unity. At low values of the potential sweep rates of ≤ 50 mV s^{-1}, the anodic and cathodic peak currents depended linearly on the potential sweep rate, as shown in Fig. 3C. This behavior indicates a surface-confined redox reaction for immobilized nickel species. From the average values of the slopes of the lines in Fig. 3C, the mean value for the surface concentration of redox species of Ni(II)/Ni(III) was obtained as

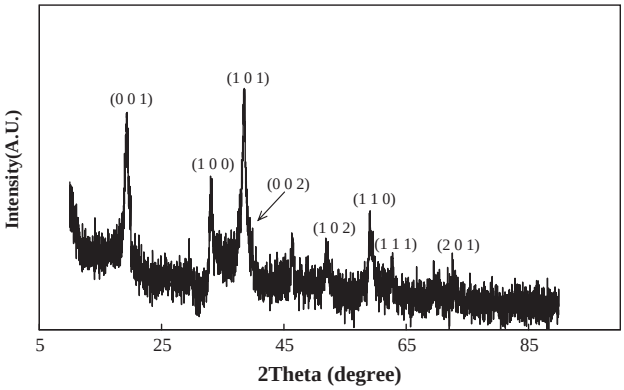

Fig. 2. Typical powder XRD pattern of the flower-like nickel oxide nanostructure.

1.40×10^{-7} mol cm^{-2}, using the following equation [54]:

$$I_p = (n^2F^2/4RT)\nu A\Gamma^* \quad (2)$$

where I_p is the peak current, n is the number of exchanged electrons, A is the geometric surface area of the electrode, and Γ^* is the surface coverage of the redox species. On the other hand, at high values of the potential sweep rates of ≥ 200 mV s^{-1}, the anodic and cathodic peak currents depend linearly on the square root of the potential sweep rate, as shown in Fig. 3D. This behavior reveals domination of a diffusion process in the redox transition at higher potential sweep rates. The redox transition of nickel-based electrodes was diffusion-controlled and it was also reported for other Ni-based electrodes [51,55], due to proton diffusion in the bulk of nickel oxide.

In order to obtain the kinetic parameters of the redox transition of nickel species at the MCPE surface, general equations for the potential sweep voltammetric responses derived by Laviron [56] were employed. These equations for peak-to-peak separation (ΔE_p) of $> 200/n$ mV are

$$E_{p,a} = E^0 + G \ln [1-\alpha_s/J] \quad (3)$$

$$E_{p,c} = E^0 + H \ln [\alpha_s/J] \quad (4)$$

$$\ln k_s = \alpha_s \ln(1-\alpha_s) + (1-\alpha_s)\ln \alpha_s - \ln(RT/nF\nu) - \alpha_s(1-\alpha_s)nF\Delta E_p/RT \quad (5)$$

where

$$G = RT/(1-\alpha_s)nF \quad (6)$$

$$H = RT/\alpha_s nF \quad (7)$$

$$J = (RT/F)(k_s/n\nu) \quad (8)$$

In these equations, k_s is an apparent rate constant for the electron jumping across the MCPE/solution interface, $E_{p,a}$ and $E_{p,c}$ are the anodic and cathodic peak potentials, respectively, and α_s is the electron transfer coefficient. Based on these equations, α_s and k_s can be determined by measuring the variation of the peak potentials with the potential sweep rate. Variations of the anodic and cathodic peak potentials with the natural logarithm of the potential sweep rate are shown in Fig. 3E. The values of E_p are proportional to ln ν at $\nu \geq 400$ mV s^{-1} and the values of α_s and k_s were obtained as 0.41 and 0.21 s^{-1}, respectively.

3.1. Electrocatalytic oxidation of choline on MCPE

Cyclic voltammograms of CPE and MCPE in the absence and presence of 10 mmol L^{-1} choline are shown in Fig. 4. In the voltammogram of CPE, a negligible anodic current related to the

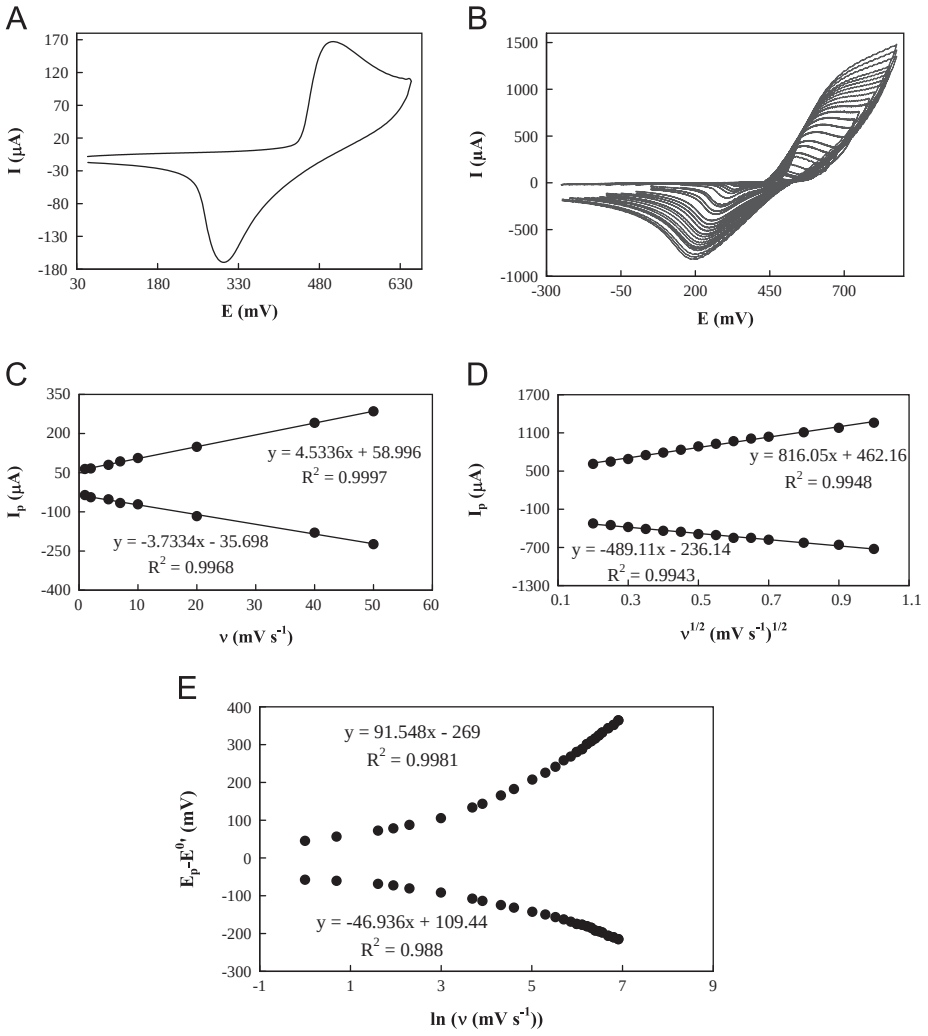

Fig. 3. (A) Typical cyclic voltammogram of MCPE recorded in 100 mM NaOH with a potential sweep rate of 50 mV s^{-1}. (B) Cyclic voltammograms of MCPE recorded in 100 mmol L^{-1} NaOH at various potential sweep rates of 1, 2, 5, 7, 10, 20, 40, 50, 75, 100, 150, 200, 250, 300, 350, 400, 450, 500, 550, 600, 650, 700, 800, 900 and 1000 mV s^{-1}. (C) Dependency of anodic and cathodic peak currents on the potential sweep rate at low values of $\lesssim$50 mV s^{-1}. (D) Dependency of anodic and cathodic peak currents on the square root of the potential sweep rate at high values of $\gtrsim$200 mV s^{-1}. (E) Variation of the anodic and cathodic peak potentials with the natural logarithm of the potential sweep rate.

electrooxidation of choline is observed, while choline was oxidized on the MCPE surface. In the presence of choline, the anodic peak current in the MCPE voltammogram increased and the cathodic peak currents slightly decreased. Therefore, choline was oxidized on the MCPE surfaces via a surface mediation electrocatalytic mechanism. Based on this mechanism, the redox transition of the nickel species

$$\mathrm{Ni(II)} \rightleftarrows \mathrm{Ni(III)} + \mathrm{e} \quad (9)$$

is coupled to the chemical oxidation of choline via the high-valence nickel species:

$$\mathrm{Ni(III)} + \mathrm{Choline} \xrightarrow{k\mathrm{cat}} \mathrm{Product} + \mathrm{Ni(II)} \quad (10)$$

In the voltammogram of MCPE in the presence of choline, both onset and peak potentials shifted toward more positive values, and also the backward current crossed the forward sweep. These behaviors which have been observed typically for alcohol electrooxidation indicate a strong interaction of choline with the MCPE surface.

Regarding the electrooxidation product of choline, it can be proposed as the oxidation of functional group(s) of choline in a single or multiple steps. Choline, as a quaternary ammonium salt, cannot be oxidized because it lacks amine hydrogen. On the other hand, as an alcohol analog, choline can be oxidized to betaine aldehyde or further to betaine [57].

Typical pseudo-steady state polarization curve for the electrooxidation of choline on the MCPE surface is shown in Fig. 5. A S-shaped plot was obtained and the electron transfer coefficient for the electrooxidation of choline (α_{Ch}) was obtained by plotting the corresponding Tafel plot. The value of α_{Ch} was obtained as 0.57, indicating a slight curvature of the potential energy barrier to the reactants.

Cyclic voltammograms of MCPE recorded in the presence of 10 mmol L^{-1} choline at different potential sweep rates (1–1000 mV s^{-1}) are shown in Fig. 6A. In these voltammograms, the anodic peak current depended linearly on the square root of the potential sweep rate, as shown in Fig. 6B. This indicates that the electrooxidation of choline is controlled by its diffusion in the bulk of the solution. Based on the following equation [54]:

$$I_{\mathrm{pa}} = (2.99 \times 10^5)\alpha_{\mathrm{Ch}}{}^{1/2} n^{3/2} A C D^{1/2} n^{1/2} \quad (11)$$

where I_{pa} is the anodic peak current, A is the electrode surface area, D is the diffusion coefficient, and C is the bulk concentration of choline, the diffusion coefficient of choline was obtained as 1.76×10^{-6} cm^2 s^{-1}. Dependency of the anodic peak potential on the natural logarithm of the potential sweep rate is shown in

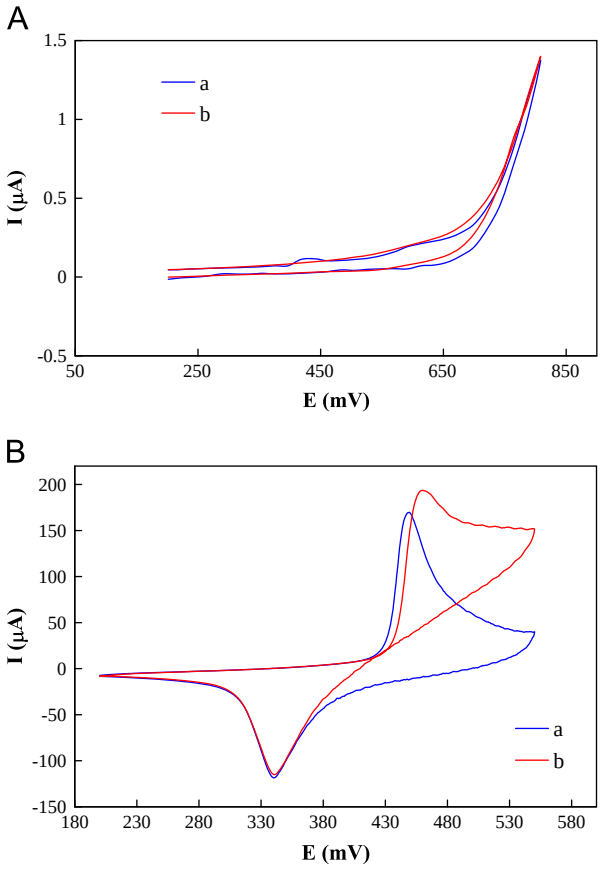

Fig. 4. Cyclic voltammograms of CPE (A) and MCPE (B) in the absence (curve a) and presence (curve b) of 10 mmol L^{-1} choline. The potential sweep rate was 50 mV s^{-1}.

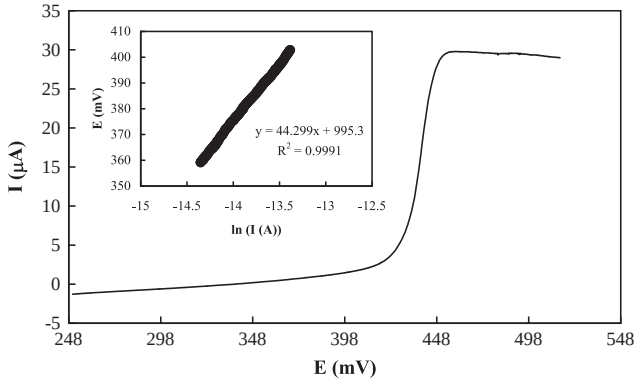

Fig. 5. Typical pseudo-steady state polarization curve for the electrooxidation of 10 mmol L^{-1} choline on the MCPE surface.

Fig. 6C. Based on this plot, and using the following equation [58],

$$E_p = (RT/2\alpha F)\ln n + \text{constant} \quad (12)$$

the electron-transfer coefficient for the electrooxidation of choline was obtained as 0.52. This value is in agreement with that obtained from Tafel plot. Based on the voltammograms presented in Fig. 6A, dependence of the current function (peak current divided by the square root of the potential sweep rate) on the square root of the potential sweep rate is presented in Fig. 6D. The current function decayed and the plot had a negative slope. This behavior further confirms the electrocatalytic nature of choline electrooxidation reaction.

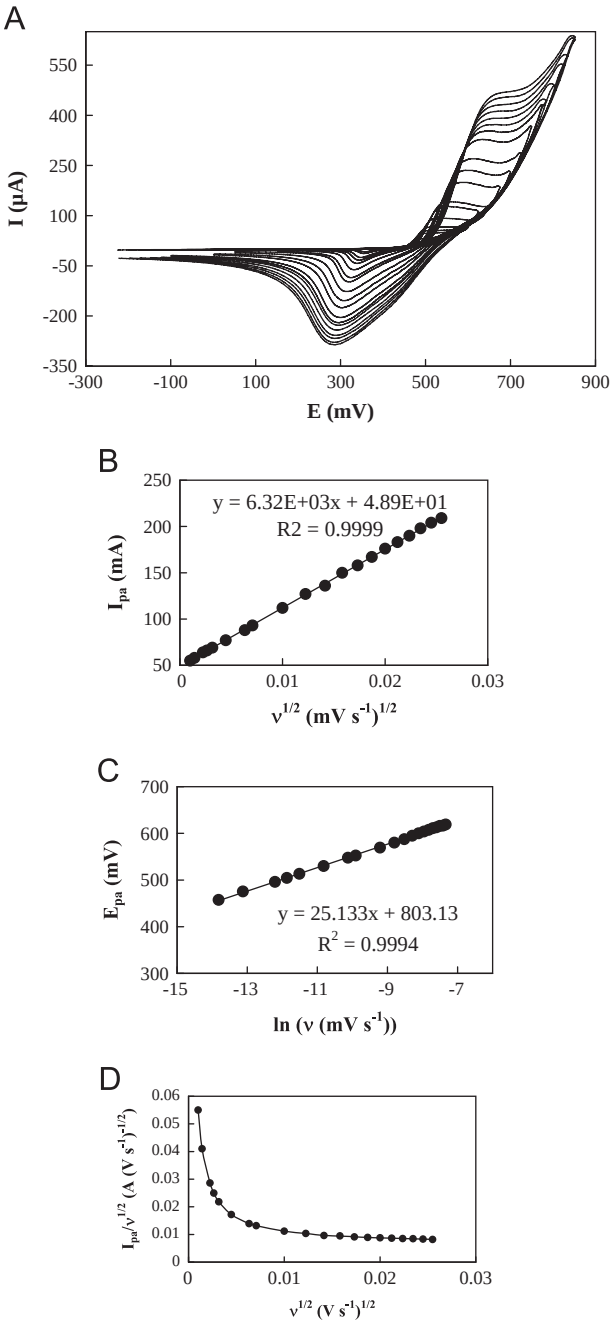

Fig. 6. (A) Cyclic voltammograms of MCPE recorded in the presence of 10 mmol L^{-1} choline at different potential sweep rates of 1, 2, 5, 7, 10, 20, 40, 50, 75, 100, 150, 200, 250, 300, 350, 400, 450, 500, 550, 600, 650, 700, 800, 900 and 1000 mV s^{-1}. (B) Dependency of the anodic peak current on the square root of the potential sweep rate. (C) Dependency of the anodic peak potential on the natural logarithm of the potential sweep rate. (D) Dependency of the current function (peak current divided by the square root of the potential sweep rate) on the square root of the potential sweep rate. The data was derived from voltammograms presented in (A).

3.2. Kinetics of electrocatalytic oxidation of choline on MCPE

In order to study the kinetics of the choline electrocatalytic oxidation by the Ni(III) active species, chronoamperometry was employed. Chronoamperograms recorded using MCPE in the absence and presence of different choline concentrations are shown in Fig. 7. The transient current decayed in a Cottrellian manner (Fig. 7, inset A) confirming the fact that the electrooxidation process was diffusion-controlled. Also, the diffusion coefficient of

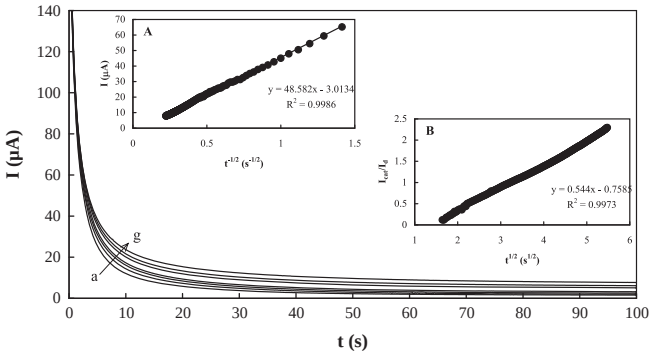

Fig. 7. Chronoamperograms for MCPE in the absence (a) and presence of 0.5 (b) 1.0 (c), 2 (d), 5 (e), 7 (f) and 10 mmol L^{-1} (g) choline. The applied potential step was 550 mV. (A) The Cottrell plot. (B) Dependency of I_{cat}/I_L on the square root of time.

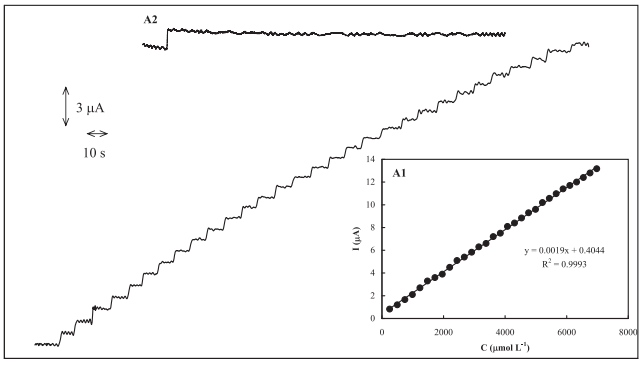

Fig. 8. Typical amperometric signals obtained during successive increments of choline using MCPE. The working potential was 550 mV. Inset A1: the calibration curve. Inset A2: an amperometric response of MCPE toward 249 μmol L^{-1} choline during a prolonged measurement of more than 25 min.

choline was obtained based on Cottrell's equation [54]:

$$I = nFAD^{1/2}C\pi^{-1/2}t^{-1/2} \quad (13)$$

as 1.62×10^{-6} cm^2 s^{-1}. This value is in close agreement with that found using cyclic voltammetry. Moreover, the catalytic rate constant of choline oxidation by Ni(III) species can also be found based on the following equation [54]:

$$I_{cat}/I_d = \gamma^{1/2}[\pi^{1/2}\mathrm{erf}(\gamma^{1/2}) + \exp(-\gamma)/\gamma^{1/2}] \quad (14)$$

where I_{cat} and I_d are the currents in the presence and absence of choline, respectively, and $\gamma = k_{cat}Ct$ is the argument of the error function, k_{cat} is the catalytic rate constant, and t is elapsed time. When $\gamma > 1.5$, $\mathrm{erf}(\gamma^{1/2})$ is almost equal to unity, and Eq. (14) is reduced to

$$I_{cat}/I_d = \gamma^{1/2}\pi^{1/2} = \pi^{1/2}(k_{cat}Ct)^{1/2} \quad (15)$$

Using the plot of I_{cat}/I_d versus $t^{1/2}$ (Fig. 7, inset B), k_{cat} is obtained as 9.46×10^3 cm^3 mol^{-1} s^{-1}. Although the arrangement of the nickel oxide flakes as a flower-like nanostructure needs permeation and diffusion of choline, its oxidation occurred with a high rate constant.

3.3. Determination of choline

Aiming at determination of choline using MCPE, amperometry was employed. Typical amperometric signals of MCPE toward the successive increments of choline concentrations are represented in Fig. 8. The corresponding calibration plot is also shown in the inset A1. The limits of detection (LOD) and quantitation (LOQ) of the procedure were calculated using the $3\sigma/b$ and $10\sigma/b$ criteria, respectively, where σ is the standard deviation of the intercept and b is the slope of the calibration curves [59]. The determined parameters for the calibration curve of choline using MCPE are displayed in Table 1. The detection limits of some different sensors for choline are presented in Table 2. An amperometric response of MCPE toward 249 μmol L^{-1} choline during a prolonged measurement of more than 25 min is shown in Fig. 8, inset A2. The amperometric response remained stable throughout the experiment (< 7% decrement in current). This indicates negligible fouling of the MCPE surface by choline and its oxidation products. Therefore, MCPE showed high stability and strong mediation properties for amperometric measurements of choline.

In order to evaluate the repeatability and reproducibility of the proposed amperometry method, three different concentrations of choline were analyzed by three independent measurements over a day (intra-day assay) and for three days (inter-day assay). The results are summarized in Table 3. In addition, 1.0 mmol L^{-1} choline was determined three times by the use of the same MCPE and the value of RSD was 0.73%. When the same determination was performed by using three MCPEs, the value of RSD was found to be 4.63%. These results confirmed that the repeatability and reproducibility of the proposed amperometry method were good.

In order to verify the stability of MCPE, consecutive cyclic voltammograms using the electrode were recorded and it was found that the peak currents changed slightly (< 4%) after 50 cycles. In addition, the electrode was stored in 100 mmol L^{-1}

Table 1
The determined parameters for the calibration curve of choline and accuracy and precision using MCPE.

Linear range/mmol L^{-1}	0.25–6.98
Sensitivity (Slope)/mA mol^{-1} L cm^{-2}	60.5
Intercept/μA cm^{-2}	12.9
R^2	0.9993
Standard error of slope (P=0.005)	9.34×10^{-5}
Standard error of intercept (P=0.005)	1.27
LOD/μmol L^{-1}	25.4
LOQ/μmol L^{-1}	84.7
RSD%	3.19
Bias%[a]	3.52

[a] The value was reported for 1.0 mM choline.

Table 2
Comparison of some various choline sensors.

Type of sensor	LOD (nmol L^{-1})	Reference
Enzymatic flow injection-amperometric detection	300	[45]
Enzymatic flow injection-dual electrode amperometric detection	100	[47]
Enzymatic flow injection-electrochemiluminescence detection	50	[60]
Enzyme-less solid-contact ion selective electrode	398	[61]
Reversed-phase HPLC with postcolumn suppression conductivity detection	19.2	[62]
Enzyme-less amperometric sensor based on flower-like nickel oxide nanostructure	25.4	This work

Table 3
Precision for assaying three concentrations of choline by the proposed amperometry method.

	C/mM		
	0.75	1.5	3.0
RSD% (intra-day assay)	3.77	3.41	3.16
RSD% (inter-day assay)	5.08	4.27	4.63

NaOH solution when it was not in use and its electrochemical reactivity was retained for at least 4 weeks.

As to investigate the selectivity of MCPE as the choline sensor, the interference effects of some common biological interferences, comprising D-glucose, dopamine, L-ascorbic acid, uric acid, L-cysteine, N-acetyl-L-cysteine, ephedrine and pseudoephedrine were evaluated when a Nafion membrane was covered on the MCPE surface (data not shown). Under the experimental conditions applied in this study, no chemical interference was observed for all these compounds due to the rejection of the diffusion of these anionic compounds by the Nafion membrane.

4. Conclusion

Nickel oxide nanoflowers were synthesized using a simple desolvation method. The method was based on the desolvation of soluble ammonia complex, which may be expanded to the other transition metal complexes using their soluble ammonia complexes. The nanoflowers were then applied to modification of a carbon paste electrode. The modified electrode was characterized electrochemically and then applied for the electrocatalytic oxidation of choline. The current generated from the oxidation of alcohol functional group was used for the quantification of choline; the modified electrode acted as an amperometric sensor for the determination of choline. When the electrode surface was covered by a layer of Nafion membrane, the interference of many anionic compounds in alkaline solutions was negligible. The modified electrode showed remarkable electrocatalytic activity, stable response and high sensitivity toward choline.

Acknowledgment

We would like to thank the Research Council of Shiraz University of Medical Sciences (Project no. 91-01-36-5409) and also the Iran National Science Foundation (INSF) for supporting this research.

References

[1] H.-J. Schafer, Topics in Current ChemistrySpringer-Verlag, Berlin Heidelberg (1987) 101–129.
[2] M. Hajjizadeh, A. Jabbari, H. Heli, A.A. Moosavi-Movahedi, A. Shafiee, K. Karimian, Anal. Biochem. 373 (2008) 337–348.
[3] N. Sattarahmady, H. Heli, A.A. Moosavi-Movahedi, Biosens. Bioelectron. 25 (2010) 2329–2335.
[4] T.R. Crompton, Battery Reference Book, 3rd ed., Reed Educational and Professional Publishing Ltd., Oxford, U.K., 2000.
[5] G.A. Niklasson, C.G. Granqvist, J. Mater. Chem. 17 (2007) 127–156.
[6] H. Heli, I. Eskandari, N. Sattarahmady, A.A. Moosavi-Movahedi, Electrochim. Acta 77 (2012) 294–301.
[7] H. Heli, F. Pourbahman, N. Sattarahmady, Anal. Sci. 28 (2012) 503–510.
[8] N. Sattarahmady, H. Heli, S.E. Moradi, Sens. Actuat. B 177 (2013) 1098–1106.
[9] H. Heli, M. Hajjizadeh, A. Jabbari, A.A. Moosavi-Movahedi, Biosens. Bioelectron. 24 (2009) 2328–2333.
[10] C. Chen, H.J. Fan, Nano Today 7 (2012) 327–343.
[11] N. Sattarahmady, H. Heli, F. Faramarzi, Talanta 82 (2010) 1126–1135.
[12] A. Casu, E. Cabrini, A. Dona, A. Falqui, Y. Diaz-Fernandez, C. Milanese, A. Taglietti, P. Pallavicini, Chem. Eur. J. 18 (2012) 9381–9390.
[13] J.C. Park, J.Y. Kim, E. Heo, K.H. Park, H. Song, Langmuir 26 (2010) 16469–16473.
[14] L. Cademartiri, G.A. Ozin, Adv. Mater. 21 (2009) 1013–1020.
[15] B.I. Kharisov, Recent Patents Nanotechnol. 2 (2008) 190–200.
[16] J. Ge, J. Lei, R.N. Zare, Nat. Nanotechnol. 7 (2012) 428–432.
[17] F. Cao, F. Zhang, R. Deng, W. Hu, D. Liu, S. Song, H. Zhang, CrystEngComm 13 (2011) 4903–4908.
[18] S.B. Kulkarni, V.S. Jamadade, D.S. Dhawale, C.D. Lokhande, Appl. Surf. Sci. 255 (2009) 8390–8394.
[19] C. Yuan, J. Li, L. Hou, L. Yang, L. Shen, X. Zhang, Electrochim. Acta. 78 (2012) 532–538.
[20] L. Kumari, W.Z. Li, Physica E 41 (2009) 1289–1292.
[21] F.S. Cai, G.Y Zhang, J. Chen, X.L. Gou, H.K. Liu, S.X. Dou, Angew. Chem. 43 (2004) 4212–4216.
[22] S. Zhang, H. Zeng, Chem. Mater. 21 (2009) 871–883.
[23] Y. Lin, T. Xie, B. Cheng, B. Geng, L. Zhang, Chem. Phys. Lett. 380 (2003) 521–525.
[24] A. Allagui, R. Wuthrich, Electrochim. Acta 58 (2011) 12–18.
[25] D. Yang, R. Wang, M. He, J. Zhang, Z. Liu, J. Phys. Chem. B 109 (2005) 7654–7658.
[26] X. Ni, Y. Zhang, D. Tian, H. Zheng, X. Wang, J. Cryst. Growth 306 (2007) 418–421.
[27] R.J. Wurtman, M. Cansev, I.H. Ulus, Handbook of Neurochemistry and Molecular Neurobiology, Springer-Verlag, Berlin Heidelberg (2010) 443–501.
[28] L.M. Sanders, S.H. Zeisel, Nutr. Today 42 (2007) 181–186.
[29] S.H. Zeisel, K.D. Costa, P.D. Franklin, E.A. Alexander, J.T. Lamont, N.F. Sheard, A. Beiser, FASEB J. 5 (1991) 2093–2098.
[30] S.H. Zeisel, J. Am. Coll. Nutr. 23 (2004) 621–626.
[31] D.M. Bowen, C.B. Smith, P. White, A.N. Davison, Brain 99 (1976) 459–496.
[32] P. Davies, A.J. Maloney, Lancet 2 (1976) 1403.
[33] K. Davis, P.A.P. Berger, Brain Acetylcholine and Neuropsychiatric Disease, Plenum Press, New York, 1979.
[34] P. Wester, S. Eriksson, A. Forsell, G. Puu, R. Adolfsson, Acta Neurol. Scand. 77 (1988) 12–21.
[35] R. Tandon, Br. J. Psychiatry 174 (1999) 7–11.
[36] T.A. Garrow, Handbook of Vitamins, 4th ed., CRC press, Boca Raton, London, New York, 2007.
[37] P.E. Potter, J.L. Meek, N.H. Neff, J. Neurochem. 41 (1983) 188–194.
[38] T. Yao, M. Sato, Anal. Chim. Acta 172 (1985) 371–375.
[39] N. Kaneda, M. Asano, T. Nagatsu, J. Chromatogr. 360 (1986) 211–218.
[40] G. Damsma, D.L. Van Bueren, B.H.C. Westerink, A.S. Horn, Chromatographia 24 (1987) 827–831.
[41] N. Tyrefors, P.G. Gillberg, J. Chromatogr. 423 (1987) 85–91.
[42] P. Van Zoonen, C. Gooijer, N.H. Velthorst, R.W. Frei, J. Gerrits, F. Flentge, J. Pharm. Biomed. Anal. 5 (1987) 485–492.
[43] A.W. Teelken, H.F. Schuring, W.B. Trieling, G. Damsma, J. Chromatogr. 529 (1990) 408–416.
[44] F. Flentge, K. Venema, T. Koch, J. Korf, Anal. Biochem. 204 (1992) 305–310.
[45] X. Qin, H. Wang, X. Wang, Z. Miao, L. Chen, W. Zhao, M. Shan, Q. Chen, Sens. Actuat. B 147 (2010) 593–598.
[46] S. Pati, M. Quinto, F. Palmisano, Anal. Chim. Acta 594 (2007) 234–239.
[47] A. Guerrieri, V. Lattanzio, F. Palmisano, P.G. Zambonin, Biosens. Bioelectron. 21 (2006) 1710–1718.
[48] M. Adamczyk, R.J. Brashear, P.G. Mattingly, P.H. Tsatsos, Anal. Chim. Acta 579 (2006) 61–67.
[49] H.C. Holmes, I. Snodgrass, R.A. R.A. Iles, Eur. J. Pediatr. 159 (2000) 198–204.
[50] H. Koc, M.H. Mar, A. Ranasinghe, J.A. Swenberg, S.H. Zeisel, Anal. Chem. 74 (2002) 4734–4740.
[51] H. Heli, A. Jabbari, S. Majdi, M. Mahjoub, A.A. Moosavi-Movahedi, S. Sheibani, J. Solid State Electrochem. 13 (2009) 1951–1958.
[52] E. Laviron, J. Electroanal. Chem. 122 (1981) 37–44.
[53] P. Daum, J.R. Lenhard, D. Rolison, R.W. Murray, J. Am. Chem. Soc. 102 (1980) 4649–4653.
[54] A.J. Bard, L.R. Faulkner, Electrochemical Methods, 2nd ed., John Wiley and Sons, New York, 2001.
[55] G. Roslonek, J. Taraszewska, Electrochim. Acta 39 (1994) 1887–1889.
[56] E. Laviron, J. Electroanal. Chem. 101 (1979) 19–28.
[57] O.N. Schuvailo, S.V. Dzyadevych, A.V. Elskaya, S. Gautier-Sauvigne, E. Csoregi, R. Cespuglio, A.P. Soldatkin, Biosens. Bioelectron. 21 (2005) 87–94.
[58] J.A. Harrison, Z.A. Khan, J. Electroanal. Chem. 28 (1970) 131–138.
[59] J.C. Miller, J.N. Miller, Statistics for Analytical Chemistry, 4th ed., Ellis-Harwood, New York (1994) 115.
[60] J. Jin, M. Muroga, F. Takahashi, T. Nakamura, Bioelectrochemistry 79 (2010) 147–151.
[61] J. Ampurdanes, G.A. Crespo, A. Maroto, M.A. Sarmentero, P. Ballester, F.X. Rius, Biosens. Bioelectron. 25 (2009) 344–349.
[62] S. Chen, V. Soneji, J. Webster, J. Chromatogr. A 739 (1996) 351–357.